

Fragmentation and energy absorption characteristics of Red, Berea and Buff sandstones based on different loading rates and water contents

Eunhye Kim^{*1}, Adriana Garcia^{2a} and Hossein Changani^{2a}

¹Department of Mining Engineering, Colorado School of Mines, 1610 Illinois Street, Golden CO 80401, U.S.A.

²Department of Mining Engineering, University of Utah, Salt Lake City UT 84102, U.S.A

(Received May 29, 2016, Revised March 27, 2017, Accepted July 8, 2017)

Abstract. Annually, the global production of construction aggregates reaches over 40 billion tons, making aggregates the largest mining sector by volume and value. Currently, the aggregate industry is shifting from sand to hard rock as a result of legislation limiting the extraction of natural sands and gravels. A major implication of this change in the aggregate industry is the need for understanding rock fragmentation and energy absorption to produce more cost-effective aggregates. In this paper, we focused on incorporating dynamic rock and soil mechanics to understand the effects of loading rate and water saturation on the rock fragmentation and energy absorption of three different sandstones (Red, Berea and Buff) with different pore sizes. Rock core samples were prepared in accordance to the ASTM standards for compressive strength testing. Saturated and dry samples were subsequently prepared and fragmented via fast and dynamic compressive strength tests. The particle size distributions of the resulting fragments were subsequently analyzed using mechanical gradation tests. Our results indicate that the rock fragment size generally decreased with increasing loading rate and water content. In addition, the fragment sizes in the larger pore size sample (Buff sandstone) were relatively smaller those in the smaller pore size sample (Red sandstone). Notably, energy absorption decreased with increased loading rate, water content and rock pore size. These results support the conclusion that rock fragment size is positively correlated with the energy absorption of rocks. In addition, the rock fragment size increases as the energy absorption increases. Thus, our data provide insightful information for improving cost-effective aggregate production methods.

Keywords: rock fragmentation sizes; dynamic and fast loading rates; hydration effect; porosity; energy absorption; split Hopkinson pressure bar (SHPB)

1. Introduction

Aggregates are among the basic raw materials used in construction, agriculture and industries that utilize chemical and metallurgical processes (Horvath 2004, Dissou and Didic 2013, Virtanti *et al.* 2013). The three main aggregate sources are crushed stone, sand and gravel. Currently, economic growth and infrastructure are being heavily impact by concrete and asphalt concrete mixtures, road stabilization and road bases. In addition, “construction sand and gravel valued at \$7 billion was produced by an estimated 4,100 companies and government agencies from approximately 6,600 operations throughout the 50 states” in the U.S. in 2014 (United States Geological Survey 2015).

Globally, the aggregate industry is confronted with numerous environmental restrictions, inconvenient geographic resource distributions and policies limiting natural sand and gravel excavation (Radzevičius *et al.* 2010). Thus, it is necessary to develop environmentally friendly extraction methods, implement better strategies for utilizing existing resources and substitute natural aggregates

in infrastructure construction (Kim *et al.* 1997, Bédérina *et al.* 2005, Kumar *et al.* 2007, Yılmaz and Tuğrul 2012). In addition, a river sand shortage exists in some area, causing the increased use of crushed sand (Kim *et al.* 1997). One major way to improve or overcome the current limitations would be to manufacture aggregates in a manner that systematically obtains predictable rock fragmentations. To do so, an effective characterization method must be used to determine the optimal loading rate and water content used in crushing methods. Aggregate industries pay little attention to identifying important parameters, such as water contents and crushing load rates, which affect rock fragmentation. Therefore, we focus on better particle size, water content and loading rate characterizations as they relate to rock fragmentation.

The particle size distributions used for material fragmentation have been an important research topic in mining and civil engineering, which has led to the development of numerous theories on the topic. Among them, an approach for predicting fragment size distributions in rocks under dynamic loading conditions was introduced (Shockey *et al.* 1974). The approach, which included a computational model, was applied to Arkansas novaculite under one-dimensional-strain dynamic load conditions. It was found that calculated and experimental novaculite fragment size distributions were in agreement, indicating that quantitative predictions of rock fragmentation could be

*Corresponding author, Assistant Professor

E-mail: ekim1@mines.edu

^aM.Sc. Student

made based on known rock properties. Another theory used for rock fragmentation predictions is the fractal theory, which has provided new opportunities for modeling rock fragmentation processes. Fractal theory addresses the scaling of hierarchical and irregular systems. Fractal algorithms are available for modeling the fragmentation of classical earth materials with fractal pore space and fractal surface. However, their experimental verification is relatively poor (Perfect 1997).

Several studies have been conducted regarding fragmentation and blastability predictions, where the term “blastability” refers to the ease with which a rock mass can be fragmented by blasting, which is closely related to fragmentation. A multivariate analysis procedure for predicting blast fragmentation using fuzzy logic and neural network methods (Kulatilake *et al.* 2010, Hudaverdi *et al.* 2011). A multivariate regression analysis was applied to develop prediction equations for estimating the mean particle size of muckpiles. However, the model only incorporated the elastic modulus of rock and other geometrical location of blasting with powder factor. Another model for predicting rock fragmentation via blasting was presented based on 16 blasting parameters without considering rock properties and conditions (Faramarzi *et al.* 2013).

For fragment size analysis, over the last 30 years, image analysis techniques have been used to measure the fragment sizes in large quarry and mining operations. Fragment size measurements of binary images occur after grey scale image segmentation (Wang 1999). Photogrammetry, also known as stereo imaging, has been adapted for use on a face shovel, which allows for fully automated measurements of muckpile rock fragmentation. More recently, 3D photogrammetry has been applied to the measurement of rock fragmentation as a result of improved technological capabilities (Noy 2012). Digital photogrammetry possesses significant advantages over image segmentation algorithms, but limitations still exist. Therefore, we chose to utilize particle sizing due to its simplicity, and apply the particle-size distribution curves attained using the U.S. standard sieve sizes.

In addition, various fields seek to understand how pore-fluids affect the mechanical properties of rocks. Dating to 1981, studies have focused on the effects of water saturation on the behavior of various rock types. Physico-chemical interactions between fluids and rock materials affect the brittle failure strength of rocks. Previously, mesoscale modeling using the Smooth Particle Hydrodynamic and Discrete Element Method approaches was used to study dynamic compaction of brittle porous materials using scanning electron microscope. It was determined that the pore fluid mitigates the interactions between grains, thus reducing grain fragmentation (Swift *et al.* 2000). Other studies have been conducted using triaxial compressive tests. The triaxial deformation of sandstones at different strain rates was used to distinguish between the physico-chemical and drainage-related effects of pore fluids in order to isolate the hydraulic weakening effect in sandstones (Duda and Renner 2012). A strength decrease due to hydraulic weakening occurred at low moisture contents in two clay-bearing sandstones. However, the authors concluded that these observations may be related to an unknown physico-chemical effect. Another triaxial

compression test study was conducted on meta-sedimentary rock samples. It concluded that peak cohesion increased by 14% and the friction angle decreased by 10% when sample states transformed from dry to hydrated conditions (Li *et al.* 2012). A study of the hydraulic weakening effect on the tensile strength and fracturing behavior of artificial Hydrocal B-11 gypsum samples showed that the tensile strength decreased by half after being immersed in water (Wong and Jong 2013). Another study evaluated the effects of full water saturation on the performance of rolling disc cutters in sandstone. The results indicated that water saturation significantly reduces the cutting forces required for Roubidoux sandstones (Abu Bakar and Gertsch 2011). A more recent study focused on the performance of radial drag picks, which operated on the same sandstone type. Those results indicated an increase in cutting forces due to increased saturation, even for saturated samples with smaller strengths (Abu Bakar and Gertsch 2013). These conflicting results emphasize the need for advancements in the fundamental comprehension of rock fragmentation processes.

In this study, we examined the effects of loading rate and water content on fragment size distribution and energy absorption in Red, Berea, and Buff sandstones containing small amounts of clay minerals (5.7-7.6%) primarily consist of quartz with different porosities with a goal of developing a better prediction fragmentation prediction system and improving aggregate manufacturing.

2. Materials and methods

2.1 Sample preparation

The Red, Berea, and Buff sandstones were prepared at a ~2 L/D ratio for fast and dynamic compressive tests as described (Kim and Changani 2016). Each sandstone block was cored with a diamond impregnated bit, cut with a diamond cutting saw blade, and the top and bottom of the sample surface were ground as flat as possible and parallel to each other within ~0.1 mm. All these sample preparation steps were performed under water supplied condition. Each sandstone sample was soaked in water for 48 h inside a vacuum chamber (25 cm/Hg) to prepare the saturated samples. In addition, half of the saturated sandstones were placed in a dry oven at 105°C for 48 h to prepare the dry samples.

2.2 Porosity and grain size measurements

A thin section analysis was conducted at TerraTek to estimate the sandstone porosities (Fig. 1) as described (Kim and Changani 2016). Three sandstone samples were soaked with a low-viscosity fluorescent red-dye epoxy resin in a vacuum to visualize porous space. The sandstones were then surfaced, mounted to standard thin section slides (24 mm × 46 mm) and ground to 30 μm thickness. The thin-sectioned sandstones were stained with potassium ferricyanide and an Alizarin Red mixture. The stained samples were photographed under plane-polarized and cross-polarized light using a Nikon polarizing microscope equipped with a Spot Insight digital camera. Void areas, which were stained pink, were considered as pore space and

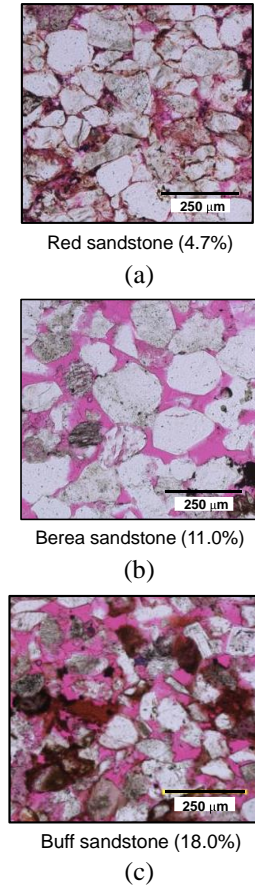


Fig. 1 The magenta epoxy is observed between framework grains. Cross-laminated Red (a), Berea (b) and Buff sandstones (c). Each percentage value indicates the porosity of the indicated sandstone. Fig. 1(a) and 1(c) were modified from our previous paper (Kim and Changani 2016). The scale bar is 250 μm

Table 1 Porosity and grain size of Red, Berea, and Buff sandstones. The value in parenthesis is the standard error of the mean (SEM, $8 \leq n \leq 20$)

Porosity and grain size	Red	Berea	Buff
Porosity (%)			
Porosity estimated from weight difference	5.6 (± 0.05)	15.8 (± 0.31)	22.6 (± 0.05)
Porosity estimated from 300-point count method	4.8	11.0	18.0
Grain size (mm)	0.13	0.15	0.1

used to estimate the porosities of the Red, Berea, and Buff sandstones. The porosity and grain size of the sandstones were estimated from a 300-point count method with the outcrop sandstone samples (Table 1).

Additionally, the porosities of the sandstones were calculated from the weight difference of the sandstone samples before and after water saturation as described (Kim and Changani 2016). The rock porosity can be calculated with the ratio of the porous rock volume filled with air and water divided by the total volume as follows (Eq. (1))

$$P = \frac{(V_w + V_a)}{(V_w + V_a + V_s)} \quad (1)$$

where V_w is the water volume, V_a is the air volume, and V_s is the volume of solid materials. The samples were dried in an oven at 105°C for 24 h. After cooling, each oven-dried sandstone was weighed, and then, the sample was immersed in distilled water for 48 h under a vacuum of 25 cmHg. After blotting with a moist cloth, the weight of the water-saturated samples was measured again. The porosities of three sandstones were calculated based on the difference of dry and saturated sandstone weights and the density of distilled water at room temperature (997 kg m^{-3}).

2.3 Fast compressive loading tests

The fast compressive tests were performed with a MTS machine under $\sim 210\text{--}265 \text{ kN s}^{-1}$ of loading rate. This chosen condition was the fastest loading rate possible for the machine, and in order to collect enough data the MTS software recorded axial force and axial LVDT position every 1000th of a second.

2.4 Dynamic compressive loading tests

Dynamic compressive tests for dry and saturated Red, Berea and Buff sandstones were conducted using a Split Hopkinson Pressure Bar (SHPB), as described (Changani *et al.* 2013, Kim and Changani 2015, Kim and Oliveira 2015, Kim and Oliveira 2016). The SHPB was comprised of an oscilloscope, projectile (striker), gas gun, laser module, two long steel rods (bars), strain gages, amplifiers and a data acquisition device (Fig. 2). The striker velocity was measured using the oscilloscope and the laser module was used to calculate loading rates. The loading rate of dynamic compressive tests was $\sim 7.0 \times 10^3\text{--}2.0 \times 10^4 \text{ MN s}^{-1}$.

2.5 Mechanical sieve analyses

After testing, all fragments were carefully collected and bagged. Each individually bagged sample was carefully placed into a previously weighed tare pan and weighed. All weights, sample weights and tare pan weights were recorded in a laboratory notebook. Gradation tests were performed on each fragmented sample using a W.S. Tyler Inc. Ro-Tap RX-29 sieve shaker machine. Each sample was gently poured into the top of the sieve stack the lid was securely placed on the stack. Each test was timed, and all samples were mechanically shaken for 5 min. Typically, soil samples are mechanically shaken for 10 min. In this case, following the recommendation of ASTM C136, samples were only shaken for 5 min to avoid further rock fragmentation (ASTM C136-14 2014). This particle sizing technique was chosen due to its simplicity, as it utilizes the particle-size distribution curves attained using the U.S. standard sieve sizes (Holtz *et al.* 2011).

2.6 Coefficient of uniformity (C_u) and coefficient of curvature (C_c)

The coefficient of uniformity (C_u) and coefficient of curvature (C_c) are well established parameters in fragmentation and particle size distribution characterization and classification. C_u and C_c were calculated using Eqs. (2)–(3)

$$C_u = \frac{D_{60}}{D_{10}} \quad (2)$$

$$C_c = \frac{D_{30}^2}{(D_{60})(D_{10})} \quad (3)$$

where D_{10} , D_{30} and D_{60} are the diameters corresponding to the percentages finer than 10, 30 and 60%, respectively.

2.7 Energy absorption in fast and dynamic rock fragmentation

In this study, absorbed energy by the sandstones was estimated from the stress pulses. The energy absorptions of dry and saturated Red, Berea and Buff sandstone, which were fragmented via fast and dynamic loading, were calculated using energy equations. Incident stress wave (W_I), transmitted stress wave (W_T) and reflected stress wave (W_R) were calculated by following equations

$$W_I = (A_b C_b / E_b) \int \sigma_I^2 dt \quad (4)$$

$$W_R = (A_b C_b / E_b) \int \sigma_R^2 dt \quad (5)$$

$$W_T = (A_b C_b / E_b) \int \sigma_T^2 dt \quad (6)$$

where A_b , C_b and E_b respectively indicate the cross sectional area of the bar, steel bar sonic velocity and Young's Modulus of the bars. In Eqs. (4)-(6), the absorbed energy by the samples (W_L), causing them to break, can be expressed by Eq. (7)

$$W_L = W_I - (W_R + W_T) \quad (7)$$

3. Results and discussion

In this paper, we analyzed Red, Berea and Buff sandstones with porosities of 4.7, 11.0 and 18.0% porosity (Fig. 1). Because these sandstones have relatively homogenous grain and pore sizes (Kim and Oliveira 2015, Kim and Oliveira 2016), they are appropriate for examining the effects of loading rate and water content on rock fragmentation and energy absorption. In addition, we investigated the effect of porosity on rock fragmentation and energy absorption based on various loading rates and water contents.

3.1 Rock fragmentation variations caused by loading rate and water content

First, we separated the rock fragments with coarse (larger than 9.56 mm) and fine (smaller than 9.56 mm) particle sizes. A 9.56 mm cutoff size is widely used to distinguish coarse and fine aggregates (Gonilho Pereira *et al.* 2009, ASTM C33-13 2013, ASTM C125-15b 2015). Table 2 shows the fine particle percentages of the Red, Berea and Buff sandstones, which are smaller than 19.05 mm. Loading rate effects on fragment size distributions

were clearly visible in the three different sandstones. For fast loading tests, the fine fragment portion to total sample weight ratio of the Red, Berea and Buff sandstones was ~16-27%. This fragment proportion increased to ~42-79% for dynamic loading tests (Table 2). These results suggest that coarse rock fragments were mainly produced by the lower loading rate (fast loading test).

Table 2 Percentage (%) value (w/w) of fine Red, Berea and Buff sandstone fragments less than 9.56 mm (3/8 inch) as compared to the total sample weight after the fast and dynamic loading tests

Loading	Status	Red	Berea	Buff
Fast	Dry	26.8% (± 1.51)	17.5% (± 1.58)	20.7% (± 1.47)
	Saturated	19.4% (± 0.67)	15.7% (± 1.77)	18.7% (± 1.02)
	P-value	< 0.001	0.249	0.154
Dynamic	Dry	42.4% (± 5.80)	55.4% (± 3.35)	70.0% (± 3.29)
	Saturated	70.1% (± 4.05)	67.0% (± 2.16)	78.7% (± 2.12)
	P-value	0.001	0.016	0.035

P-values were obtained using Student's one-tailed *t*-test. (\pm) values indicate the standard error of the mean (SEM, $3 \leq n \leq 11$). Statistically significant p-values (<0.05) between the dry and saturated samples are indicated in bold

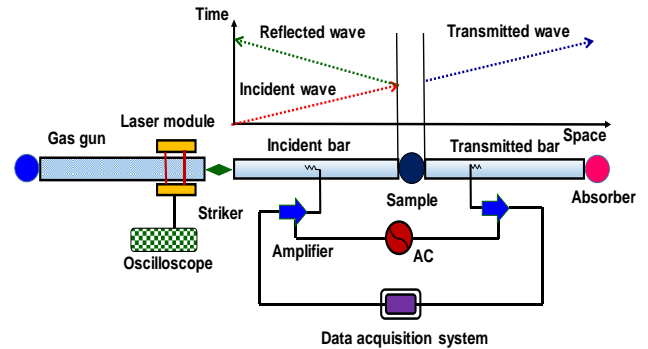


Fig. 2 Schematic diagram of the Split Hopkinson Pressure Bar (SHPB) system modified from Kim and Changani (2016)

Table 3 Summary of C_u and C_c values from the coarse and fine fragments of Red, Berea and Buff sandstones obtained via fast and dynamic loading tests

Loading	Status	Red		Berea		Buff	
		C_u	C_c	C_u	C_c	C_u	C_c
Fast	Dry	9.11 (± 0.79)	2.24 (± 0.31)	13.71 (± 3.82)	6.69 (± 1.86)	13.47 (± 1.65)	5.51 (± 1.13)
	Saturated	6.18 (± 0.42)	3.01 (± 0.27)	10.00 (± 2.80)	5.57 (± 1.46)	17.73 (± 6.39)	7.99 (± 2.98)
	P-value	0.007	0.094	0.457	0.653	0.543	0.464
Dynamic	Dry	13.42 (± 4.07)	2.11 (± 0.20)	96.14 (± 15.48)	1.66 (± 0.61)	74.44 (± 16.79)	1.09 (± 0.68)
	Saturated	58.98 (± 8.42)	1.30 (± 0.37)	28.41 (± 11.00)	0.19 (± 0.06)	37.25 (± 6.04)	0.34 (± 0.11)
	P-value	< 0.001	0.002	0.011	0.106	0.037	0.248

P-values were obtained using Student's two-tailed *t*-test. (\pm) values indicate the standard error of the mean (SEM, $3 \leq n \leq 11$). Statistically significant p-values (<0.05) between the dry and saturated samples are indicated in bold

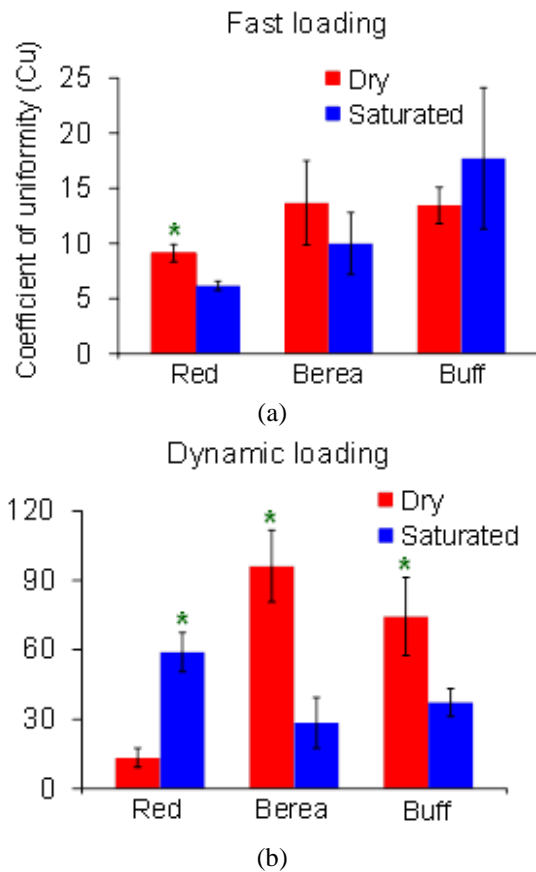


Fig. 3 Effects of the water content and loading rate on C_u (coefficient of uniformity) using whole fragments of Red, Berea and Buff sandstones. $P < 0.05$ via Student's two-tailed t -test ($3 \leq n \leq 11$). Error bars show SEM

In addition, water content effects on fragment size distributions were exhibited in the Red, Berea and Buff sandstones. The water effect was more obvious for the dynamic loading tests. As a result, coarse rock fragments were generated more often for the dry sandstones versus the saturated sandstones in dynamic loading tests. However, the rock fragmentation difference between the dry and saturated samples in the fast loading test was only ~7% in the Red sandstone and differences were statistically negligible in the Berea and Buff sandstones (Table 2). Our data support the conclusion that the water content effect on rock fragmentation is greater when the loading rate is faster (dynamic loading tests), and increased sandstone water content reduces the rock fragment size.

The coefficient of uniformity (C_u) and coefficient of curvature (C_c) are well-established parameters that are used to characterize and classify geomaterial fragment size distributions. Therefore, we utilized C_u and C_c values to investigate water and loading rate effects on fragmentation. C_u can represent the degree of rock fragment uniformity, so lower C_u values indicate more homogenous rock fragments. As results, the C_u values from the fast loading tests ranged from ~6.2-17.7, whereas dynamic loading test values were ~13.4-96.1 (Table 3 and Fig. 3). This suggests that more uniform rock fragments can be produced via lower (fast) loading conditions.

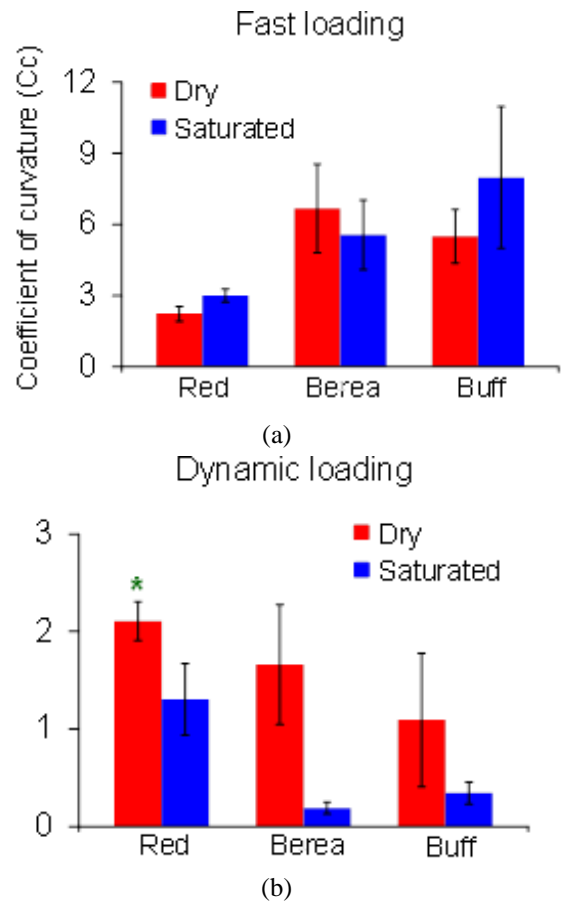


Fig. 4 Effects of the water content and loading rate on C_c (coefficient of curvature) using whole fragments of Red, Berea and Buff sandstones. $P < 0.05$ using Student's two-tailed t -test ($3 \leq n \leq 11$). Error bars show SEM

In addition, the water effect on C_u was more obvious in the dynamic loading tests. In fast loading tests, the water effect on C_u was statistically insignificant between the dry and saturated Berea and Buff sandstones, but a significant water effect was observed in the Red sandstone (Fig. 3(a)). The water effect on rock fragmentation uniformity during the dynamic loading test was significant, as C_u value differences were exhibited between the dry and saturated samples of all three sandstones (Fig. 3(b)). However, the water effect on C_u varied depending on the porosity of the sandstones in the dynamic loading tests.

In our study, the water effect on C_u was more drastic in small pore size sandstones, such as the Red sandstone with fast loading. In higher porosity sandstones such the Berea and Buff sandstones, the water effect on C_u was not significant. In the dynamic loading tests, the C_u value of Red sandstone was significantly lower in the dry state, whereas the C_u values of Berea and Buff sandstones were greater in the saturated state. These results suggest that the effect of water content on rock fragmentation differs based on porosity. In addition, our data provide important information regarding the generation of a more homogeneous sandstone particle size. Overall C_u values in fast loading tests were lower than those in dynamic loading tests. Thus, fast loading conditions are favorable for producing more uniform fragments.

Table 4 Summary of C_u and C_c values obtained via the fine fragment analysis of the Red, Berea and Buff sandstones during fast and dynamic loading tests

Loading	Status	Red		Berea		Buff	
		C_u	C_c	C_u	C_c	C_u	C_c
Fast	Dry	52.47 (± 2.77)	4.74 (± 0.38)	29.79 (± 1.07)	0.19 (± 0.01)	70.67 (± 13.91)	0.13 (± 0.03)
	Saturated	54.51 (± 2.51)	3.59 (± 0.21)	17.90 (± 4.56)	0.36 (± 0.14)	68.97 (± 11.59)	0.09 (± 0.02)
	P-value	0.598	0.02	0.082	0.62	0.928	0.33
Dynamic	Dry	27.03 (± 2.67)	3.77 (± 0.55)	16.30 (± 3.36)	0.36 (± 0.08)	21.77 (± 4.14)	0.46 (± 0.14)
	Saturated	21.01 (± 2.24)	0.36 (± 0.03)	4.53 (± 0.51)	0.93 (± 0.09)	13.58 (± 2.28)	0.41 (± 0.03)
	P-value	0.120	<0.001	<0.001	<0.001	0.106	0.668

P-values were obtained using Student’s two-tailed t -test. (\pm) values indicate the standard error of the mean (SEM, $3 \leq n \leq 11$). Statistically significant p-values (<0.05) between the dry and saturated samples are indicated in bold

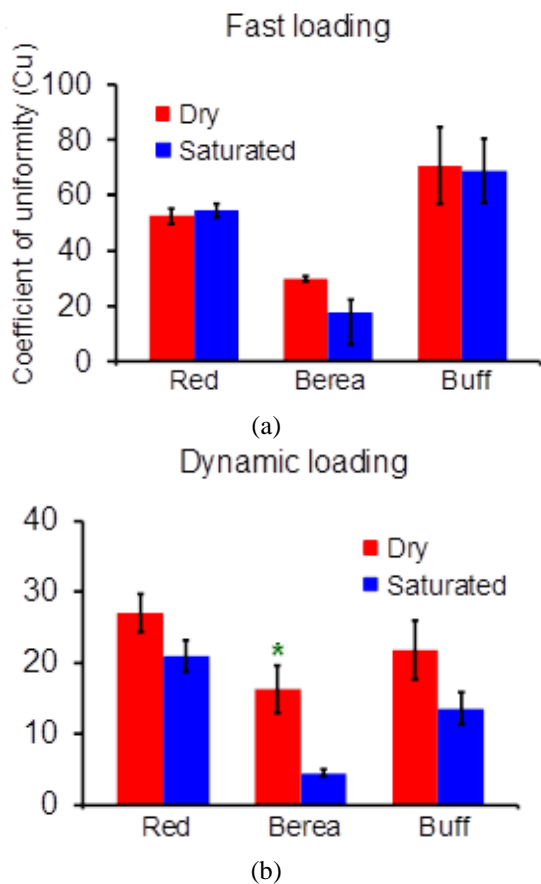


Fig. 5 Effects of the water content and loading rate on C_u (coefficient of uniformity) in the fine fragments of the Red, Berea and Buff sandstones. $P < 0.05$ using Student’s two-tailed t -test ($3 \leq n \leq 11$). Error bars indicate SEM

A relative higher C_c value is desirable, as C_c value indicates that the fragments are poorly graded, which mean fewer fragment sizes are abundant, suggesting a more uniform fragment size. First, the overall C_c values were greater during fast loading tests than dynamic loading tests (Fig. 4), suggesting that fast loading is the more effective technique for sandstone aggregate applications. The water

effects on C_c were not observed during fast loading tests (Fig. 4(a)), whereas the C_c value decreased with increasing rock porosity and water content in the dynamic loading tests (Fig. 4(b)).

3.2 Effects of water, loading rate and porosity on rock fragmentation obtained via fine fragment analysis

In some cases, fine particles are exclusively desired for aggregate applications, especially in certain concrete mixes. Thus, we examined fine fragment size distributions for sandstone fragments smaller than 9.56 mm. In contrast to the C_u values obtained during the whole fragment analysis, the C_u values obtained during the fine fragment analysis were relatively higher for the fast loading tests than the dynamic tests (Table 4). The C_u values from the fast loading tests ranged from ~ 17.9 - 70.7 , whereas the values from the dynamic tests were between ~ 4.5 - 27.0 . Note that, unlike the whole fragment analysis, water effects on C_u were not obvious in smaller (Red) and larger (Buff) porosity sandstones for either loading condition (Fig. 5). However, the water effect on C_u in the Berea sandstone (intermediate porosity) was significant for dynamic loading tests, as the

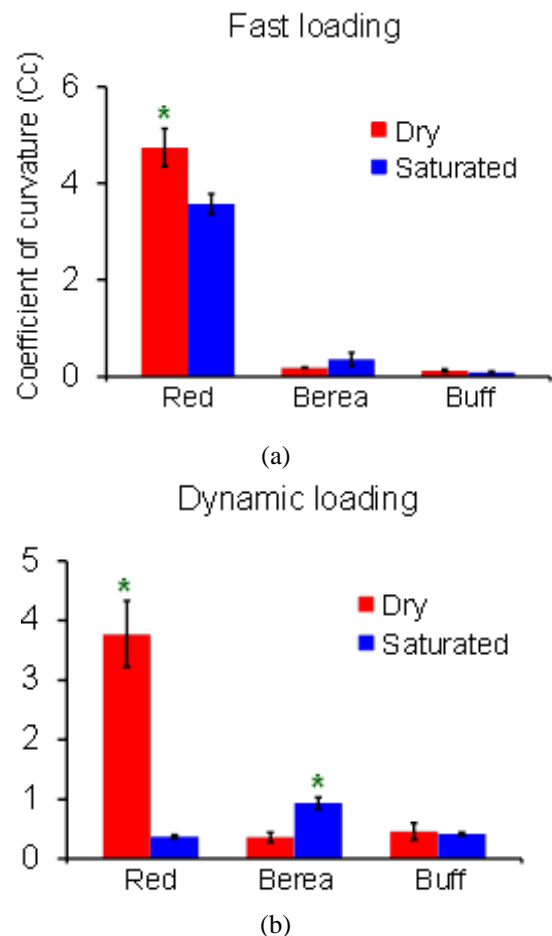


Fig. 6 Effects of the water content and loading rate on C_c (coefficient of curvature) during the fine fragment analyses of the Red, Berea and Buff sandstones. $P < 0.05$ using Student’s two-tailed t -test ($3 \leq n \leq 11$). Error bar is SEM

C_u value was statistically greater in dry state than saturated sample (Fig. 5).

To date, we do not fully understand why the water effect on the C_u values obtained during the fine fragment analysis was meaningful only in the Berea sandstone under a dynamic loading rate.

The results support the evidence that dynamic tests generate smaller rock fragments as a dynamic loading increases crack branches or bifurcations when compared with a fast loading condition.

The loading rate effect on C_c was not significant during the fine fragment analysis, except for the Red sandstone. However, the porosity effect was significant, as the C_c values dramatically decreased in the Berea and Buff sandstones (Fig. 6). In addition, significant water content effects on C_c were revealed in the Red sandstone during fast and dynamic loading conditions, as well as in the Berea sandstone under dynamic loading conditions. These data indicate that the water content, loading rate and porosity effects on the C_c values differ between the whole and fine fragment analysis. Thus, we suggest that the water content, porosity and loading rate are considered based on expected fragment sizes and their applications during sandstone aggregate production via crushing or breaking sandstone. Our results provide information about how rock fragmentation can be affected with porosity, water content, mechanical force applied. Thus, rock porosity and its water content should be considered in rock aggregate production processes. In other words, when producing aggregates, mechanical forces applied to rocks should be adjusted with rock porosity and its water content.

3.3 Energy absorption changes due to loading rate and water content

Experimental and theoretical size distributions produced by dynamic fragmentation have been the focus of several studies (Grady 2008, Grady 2010, Hogan *et al.* 2012, Hogan *et al.* 2013, Ramesh *et al.* 2015). One study focused on rock fracture loading rate effects and used the Split Hopkinson Pressure Bar (SHPB) to apply wedge loading to a short-rod rock fracture specimen (Zhang *et al.* 1999, Zhang *et al.* 2000). Until then, most loading rate research related to rock destruction was limited to the influences of the loading rate on rock strength. In order to understand the effect of the loading rate on rock fragmentation, it is important to relate both the fragment sizes and fragmentation energy to the loading rate (Zhang *et al.* 1999). Thus, energy absorption variations linked to water content, loading rates and rock porosity values can offer useful insights regarding rock fragmentation and size distributions.

Grady (2008) proposed energy-based dynamic fragmentation theory that aided in understanding the failure of brittle solids (Grady 2008). Consistent with his idea, our results of fragment size distribution obtained from dynamic loading tests exhibit that the size distribution is exponential or exponential-like. Previous study reported that the influence of dynamic loading on the rock fragment size depended on the accumulation of increased shear deformation energy during the fracture moment (Qi *et al.* 2009). This increase of shear deformation energy was due

Table 5 Energy absorptions of dry and saturated Red, Berea and Buff sandstones under fast and dynamic loading rates

Loading	Status	Red	Berea	Buff
Fast	Dry	28.4 (\pm 1.66)	17.4 (\pm 0.58)	13.2 (\pm 0.56)
	Saturated	17.6 (\pm 0.80)	10.6 (\pm 0.22)	8.75 (\pm 0.14)
	P-value	< 0.001	< 0.001	< 0.001
Dynamic	Dry	18.1 (\pm 1.11)	7.46 (\pm 2.92)	5.61 (\pm 0.71)
	Saturated	10.5 (\pm 0.54)	9.13 (\pm 2.04)	7.87 (\pm 1.79)
	P-value	< 0.001	0.656	0.272

P-values were obtained using Student's two-tailed *t*-test. (\pm) values indicate SEM ($3 \leq n \leq 11$). Statistically significant p-values (< 0.05) between the dry and saturated samples are indicated in bold. Unit: N·m

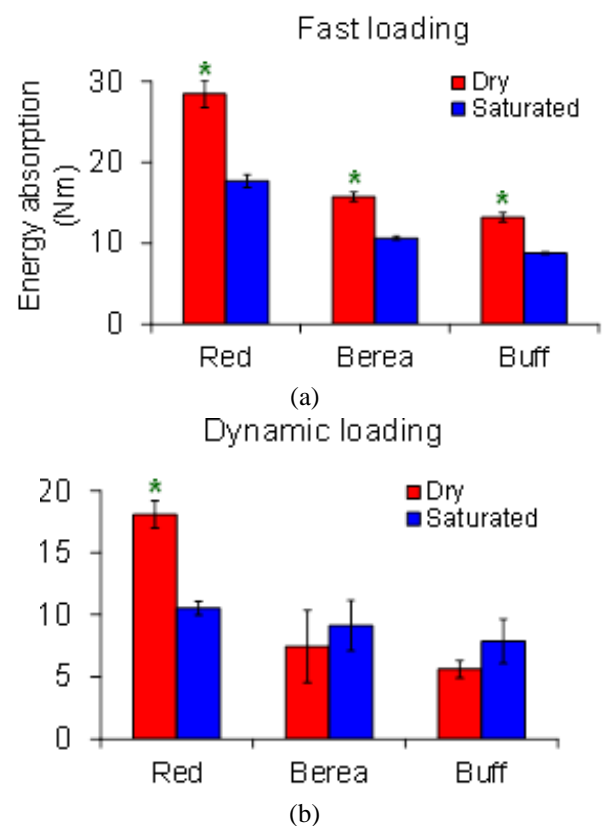


Fig. 7 Energy absorption comparison between dry and saturated Red, Berea and Buff sandstones during the fast (a) and dynamic (b) loading tests. * $P < 0.05$ used Student's two-tailed *t*-test ($3 \leq n \leq 11$). Error bars indicate SEM

to the strength increase originating from the stress state change, accumulation of plastic deformation and strain rate (Qi *et al.* 2009). Thus, energy absorption in geomaterials can be related to fragmentation size distribution due to stress wave loading (Lundberg 1976).

In general, more energy was absorbed during the fast loading tests than during the dynamic tests. The range of energy absorption values during the fast loading tests was ~ 8.8 - 28.4 , these values ranged from ~ 5.6 - 18.1 during the dynamic loading tests (Table 5). In addition, the energy

Table 6 Summary of water content and loading rate effects on rock fragmentation

Method	Parameter	Porosity	Water (dry vs. saturated) and loading rate (fast vs. dynamic)
Mechanical sieve analysis	Larger than 9.58 mm	Small (~ 5%)	Saturated and fast
		Large (> 10%)	Fast (insignificant water effect)
Whole fragment analysis	Lower C_u	Small (~ 5%)	Saturated and fast
		Large (> 10%)	Dry and fast
	Higher C_c	Small (~ 5%)	Saturated and fast
		Large (> 10%)	Fast (insignificant water effect)
Fine fragment analysis	Lower C_u	Small (~ 5%)	Dynamic (insignificant water effect)
		Large (> 10%)	Saturated and dynamic
	Higher C_c	Small (~ 5%)	Dry and fast
		Large (> 10%)	Dynamic (insignificant water effect)
Energy absorption (higher)		Small (~ 5%)	Dry and fast
		Large (> 10%)	Dry and fast

Based on the sandstone porosity, water content and loading rate are suggested for the production of larger rock fragments

absorption was greater under dry rock conditions, especially for fast loading conditions (Fig. 7(a)). Additionally, the smaller porosity rock (Red sandstone) absorbed more energy than the larger porosity sandstones (Berea and Buff) based on the same loading rate and water content (Fig. 7 and Table 5).

In summary, the energy absorption in fractured sandstones increased as the pore size (Red>Berea and Buff), water content (dry>saturated) and loading rate decreased (fast>dynamic). These conditions are also more favorable for generating larger sandstone fragments. Based on the results, we conclude that when larger fragments were generated, more energy was absorbed except Red sandstone under the fast loading condition. Conversely, less energy was absorbed when finer fragments were produced. To date we do not fully understand why Red sandstone at the fast loading tests deviates from the characteristic trend although we suspect the combined effects of water content, loading rate, and porosity on the Red sandstone fragmentation. Thus, further work will focus on detailed mechanism of rock fragmentation including rock fracture processes with the changes of water content and loading rate. In conclusion, we summarized water content and loading rate effects for each parameter (Table 6). It is noticeably that the loading rate should be set based on the desired fragment production.

4. Conclusions

The water content and loading rate effects on fragment size distributions and energy absorption were examined for three different sandstones (Red, Berea and Buff) with different porosities. The primary conclusions of this study are as follows: (1) sandstone fragment size decreased as loading rate increased; (2) the water contents effects on Cu

were greater for the dynamic tests, versus the fast loading tests, during the whole fragment analysis; (3) the rock porosity effects on C_c were significant for the dynamic loading tests during the fine fragment analysis; and (4) the fractured sandstone energy was greater when the pore size was smaller, water content was lower and loading rate was slower. Our findings provide insights that can be used to develop a systematic method for categorizing fragment size distribution based on water content, loading rate and rock porosity, contributing to advancements in aggregate applications and production.

Acknowledgments

The authors wish to thank Michael A. Stine and Davi Bastos Martins de Oliveira for their technical assistance.

References

- Abu Bakar, M.Z. and Gertsch, L.S. (2011), "Saturation effects on disc cutting of sandstone", *Proceedings of the 45th US Rock Mechanics/Geomechanics Symposium*, San Francisco, California, U.S.A., June.
- Abu Bakar, M.Z. and Gertsch, L.S. (2013), "Evaluation of saturation effects on drag pick cutting of a brittle sandstone from full scale linear cutting tests", *Tunn. Undergr. Sp. Technol.*, **34**, 124-134.
- ASTM C125-15b (2015), *Standard Terminology Relating to Concrete and Concrete Aggregates*, ASTM International.
- ASTM C136-14 (2014), *Standard Test Methods for Sieve Analysis of Fine and Coarse Aggregates*, ASTM International.
- ASTM C33-13 (2013), *Standard Specification for Concrete Aggregates*, ASTM International.
- Bédérina, M., Khenfer, M.M., Dheilily, R.M. and Quéneudec, M. (2005), "Reuse of local sand: effect of limestone filler proportion on the rheological and mechanical properties of different sand concretes", *Cement Concrete Res.*, **35**(6), 1172-1179.
- Changani, H., Young, A. and Kim, E. (2013), "Effect of L/D ratio on dynamic response of aluminum 7076 and the natural Motoqua quartzite sandstone in Saint George, UT using Split Hopkinson Pressure Bar (SHPB)", *Proceedings of the 47th US Rock Mechanics/Geomechanics Symposium*, San Francisco, California, U.S.A., June.
- Dissou, Y. and Didic, S. (2013), *Infrastructure and Growth*, Springer International Publishing.
- Duda, M. and Renner, J. (2012), "The weakening effect of water on the brittle failure strength of sandstone", *Geophys. J.*, **192**(3), 1091-1108.
- Faramarzi, F., Mansouri, H. and Ebrahimi Farsangi, M.A. (2013), "A rock engineering systems based model to predict rock fragmentation by blasting", *J. Rock Mech. Min. Sci.*, **60**, 82-94.
- Gonilho Pereira, C., Castro-Gomes, J. and Pereira De Oliveira, L. (2009), "Influence of natural coarse aggregate size, mineralogy and water content on the permeability of structural concrete", *Construct. Build. Mater.*, **23**(2), 602-608.
- Grady, D.E. (2008), "Fragment size distributions from the dynamic fragmentation of brittle solids", *J. Impact Eng.*, **35**(12), 1557-1562.
- Grady, D.E. (2010), "Length scales and size distributions in dynamic fragmentation", *J. Fract.*, **163**(1), 85-99.
- Hogan, J.D., Rogers, R.J., Spray, J.G. and Boonsue, S. (2012), "Dynamic fragmentation of granite for impact energies of 6-

- 28", *J. Eng. Fract. Mech.*, **79**, 103-125.
- Hogan, J.D., Spray, J.G., Rogers, R.J., Vincent, G. and Schneider, M. (2013), "Dynamic fragmentation of planetary materials: Ejecta length quantification and semi-analytical modelling", *J. Impact Eng.*, **62**, 219-228.
- Holtz, R.D., Kovacs, W.D. and Sheahan, T.C. (2011), *An Introduction to Geotechnical Engineering*, Prentice-Hall, New Jersey, U.S.A.
- Horvath, A. (2004), "Construction materials and the environment", *Annu. Rev. Environ. Res.*, **29**(1), 181-204.
- Hudaverdi, T., Kulatilake, P.H.S.W. and Kuzu, C. (2011), "Prediction of blast fragmentation using multivariate analysis procedures", *J. Numer. Anal. Meth. Geomech.*, **35**(12), 1318-1333.
- Kim, E. and Changani, H. (2015), "Study of dynamic mechanical behavior of aluminum 7075-T6 with respect to diameters and L/D ratios using Split Hopkinson Pressure Bar (SHPB)", *Struct. Eng. Mech.*, **55**(4), 857-869.
- Kim, E. and Changani, H. (2016), "Effect of water saturation and loading rate on the mechanical properties of Red and Buff sandstones", *J. Rock Mech. Min. Sci.*, **88**, 23-28.
- Kim, E. and Oliveira, D.B.M.D. (2015), "The effects of water saturation on dynamic mechanical properties in red and buff sandstones having different porosities studied with Split Hopkinson Pressure Bar (SHPB)", *App. Mech. Mater.*, 752-753, 784-789.
- Kim, E. and Oliveira, D.B.M.D. (2016), "The water saturation effects on dynamic tensile strength in red and buff sandstones studied with Split Hopkinson Pressure Bar (SHPB)", *Proceedings of the International Conference on Advanced Materials, Structures and Mechanical Engineering*, Incheon, South Korea, May.
- Kim, J.K., Lee, C.S., Park, C.K. and Eo, S.H. (1997), "The fracture characteristics of crushed limestone sand concrete", *Cement Concrete Res.*, **27**(11), 1719-1729.
- Kulatilake, P.H.S.W., Qiong, W., Hudaverdi, T. and Kuzu, C. (2010), "Mean particle size prediction in rock blast fragmentation using neural networks", *Eng. Geol.*, **114**(3), 298-311.
- Kumar, P.S., Mannan, M.A., Kurian, V.J. and Achuytha, H. (2007), "Investigation on the flexural behaviour of high-performance reinforced concrete beams using sandstone aggregates", *Build. Environ.*, **42**(7), 2622-2629.
- Li, D., Wong, L.N.Y., Liu, G. and Zhang, X. (2012), "Influence of water content and anisotropy on the strength and deformability of low porosity meta-sedimentary rocks under triaxial compression", *Eng. Geol.*, **126**, 46-66.
- Lundberg, B. (1976), "A split Hopkinson bar study of energy absorption in dynamic rock fragmentation", *J. Rock Mech. Min. Sci. Geomech. Abstr.*, **13**(6), 187-197.
- Noy, M.J. (2012), *Automated Rock Fragmentation Measurement with Close Range Digital Photogrammetry*, CRC Press.
- Perfect, E. (1997), "Fractal models for the fragmentation of rocks and soils: A review", *Eng. Geol.*, **48**(3-4), 185-198.
- Qi, C., Wang, M. and Qian, Q. (2009), "Strain-rate effects on the strength and fragmentation size of rocks", *J. Impact Eng.*, **36**(12), 1355-1364.
- Radzevičius, R., Velegrakis, A.F. and Bonne, W. (2010), "Marine aggregate extraction regulation in EU member states", *J. Coastal Res.*, 15-37.
- Ramesh, K.T., Hogan, J.D., Kimberley, J. and Stickle, A. (2015), "A review of mechanisms and models for dynamic failure, strength, and fragmentation", *Planet. Space Sci.*, **107**, 10-23.
- Shockey, D.A., Curran, D.R., Seaman, L., Rosenberg, J.T. and Petersen, C.F. (1974), "Fragmentation of rock under dynamic loads", *J. Rock Mech. Min. Sci. Geomech. Abstr.*, **11**(8), 303-317.
- Swift, R.P., Hagelberg, C.R., Carney, T.C., Greening, D. and Hiltl, M. (2000), *Modeling Stress-Induced Damage from Impact Recovery Experiments*, Los Alamos National Laboratory, EES Division, Los Alamos, NM 87545, New Orleans, Louisiana, U.S.A.
- United States Geological Survey (2015), *Mineral Commodity Summaries*, January 2015
- Virtanti, A.A., Suriamihardja, D.A., Saleh, P. and Ria, I.U. (2013), "Supply and demand of jemberang river aggregate using multiple regression model", *J. Innov. Appl. Stud.*, **3**(3), 774-780.
- Wang, W. (1999), "Image analysis of aggregates", *Comput. Geosci.*, **25**(1), 71-81.
- Wong, L.N.Y. and Jong, M.C. (2013), "Water saturation effects on the Brazilian tensile strength of gypsum and assessment of cracking processes using high-speed video", *Rock Mech. Rock Eng.*, **47**(4), 1103-1115.
- Yılmaz, M. and Tuğrul, A. (2012), "The effects of different sandstone aggregates on concrete strength", *Construct. Build. Mater.*, **35**, 294-303.
- Zhang, Z.X., Kou, S.Q., Yua, J., Yu, Y., Jianga, L.G. and Lindqvist, P.A. (1999), "Effects of loading rate on rock fracture", *J. Rock Mech. Min. Sci.*, **36**(5), 597-611.
- Zhang, Z.X., S.Q. Kou, L.G. Jiang and Lindqvist, P.A. (2000), "Effects of loading rate on rock fracture: Fracture characteristics and energy partitioning", *J. Rock Mech. Min. Sci.*, **37**(5), 745-762.